Human Molecular Genetics, 2010, Vol. 19, No. 20 **3895–3905**
doi:10.1093/hmg/ddq300
Advance Access published on July 16, 2010

Early heart failure in the SMNΔ7 model of spinal muscular atrophy and correction by postnatal scAAV9-SMN delivery

Adam K. Bevan[1,3,†], Kirk R. Hutchinson[2,5,†], Kevin D. Foust[1], Lyndsey Braun[1], Vicki L. McGovern[4], Leah Schmelzer[1], Jennifer G. Ward[6], Jeffrey C. Petruska[7,8], Pamela A. Lucchesi[2], Arthur H.M. Burghes[3,4] and Brian K. Kaspar[1,3,4,*]

[1]Department of Gene Therapy, The Research Institute and [2]The Center for Cardiovascular and Pulmonary Research and The Heart Center, Nationwide Children's Hospital, Columbus, OH 43205, USA, [3]Integrated Biomedical Sciences Graduate Program and [4]Department of Molecular and Cellular Biochemistry, The Ohio State University, Columbus, OH 43210, USA, [5]Department of Pharmacology and Experimental Therapeutics, Louisiana State University Health Sciences Center, New Orleans, LA, USA, [6]Specialty VETPATH, Seattle, WA 98103, USA, [7]Department of Anatomical Sciences & Neurobiology and [8]Kentucky Spinal Cord Injury Research Center, Department of Neurological Surgery, University of Louisville, Louisville, KY 40292, USA

Received April 27, 2010; Revised and Accepted July 12, 2010

Proximal spinal muscular atrophy (SMA) is a debilitating neurological disease marked by isolated lower motor neuron death and subsequent atrophy of skeletal muscle. Historically, SMA pathology was thought to be limited to lower motor neurons and the skeletal muscles they control, yet there are several reports describing the coincidence of cardiovascular abnormalities in SMA patients. As new therapies for SMA emerge, it is necessary to determine whether these non-neuromuscular systems need to be targeted. Therefore, we have characterized left ventricular (LV) function of SMA mice (*SMN2*+/+; SMNΔ7+/+; *Smn*−/−) and compared it with that of their unaffected littermates at 7 and 14 days of age. Anatomical and physiological measurements made by electrocardiogram and echocardiography show that affected mouse pups have a dramatic decrease in cardiac function. At 14 days of age, SMA mice have bradycardia and develop a marked dilated cardiomyopathy with a concomitant decrease in contractility. Signs of decreased cardiac function are also apparent as early as 7 days of age in SMA animals. Delivery of a survival motor neuron-1 transgene using a self-complementary adeno-associated virus serotype 9 abolished the symptom of bradycardia and significantly decreased the severity of the heart defect. We conclude that severe SMA animals have compromised cardiac function resulting at least partially from early bradycardia, which is likely attributable to aberrant autonomic signaling. Further cardiographic studies of human SMA patients are needed to clarify the clinical relevance of these findings from this SMA mouse.

INTRODUCTION

Proximal spinal muscular atrophy (SMA) is a devastating disease that affects 1 in 5000–10 000 newborns and is one of the leading genetic causes of infant death in the USA (1). SMA is caused by a deletion or mutation of the survival motor neuron-1 (*SMN1*) gene along with retention of the *SMN2* gene (2,3). *SMN1* and *SMN2* essentially differ by a single nucleotide in exon 7 which disrupts the splicing of SMN2 pre-mRNA such that the majority of the mRNA from *SMN2* lacks exon 7 which produces a protein that is ineffective at oligomerization and thus gets rapidly degraded as it

*To whom correspondence should be addressed at: The Research Institute at Nationwide Children's Hospital, The Ohio State University, 700 Children's Drive, WA3022, Columbus, OH 43205, USA. Tel: +1 6147225085; Fax: +1 6143555247; Email: brian.kaspar@nationwidechildrens.org
†The authors wish it to be known that, in their opinion, the first two authors should be regarded as joint First Authors.

does not incorporate into the SMN complex (4–13). The SMN genes express SMN ubiquitously in all cells; however, high levels of SMN appear to be particularly important for motor neurons as depletion of SMN results in the dysfunction and death of lower motor neurons, characteristic of SMA; the exact mechanism or reason for this selectivity is unknown (3). The copy number of *SMN2* and the amount of SMN correlate with phenotypic severity with mild patients generally having a high copy number of *SMN2* and higher levels of SMN protein (4,5,14,15).

The most severe form of SMA is type 0 with clear symptoms at birth, followed by type 1 SMA patients who usually die within 2 years. As these patients have the lowest SMN levels as well as *SMN2* copy number, they are the most likely to show defects in cells other than the motor neuron. A few key studies regarding SMA patients have implicated the involvement of cardiovascular and autonomic nervous systems. An early study reported symptomatic cardiac involvement in patients with a milder form of SMA, although the population studied was not genetically defined (16). A retrospective study of type 1 SMA patients identified that 15 of 63 SMA patients experienced symptomatic bradycardia (17). Another report showed an increase in the coincidence of congenital heart defects in very severe type 0 SMA patients. The most common abnormality noted was a septal defect in the atria and/or ventricles (18). Others performed a battery of autonomic tests on type 1 SMA patients and reported a sympathetic-vagal imbalance, fluctuation of blood pressure and abnormal skin responses to temperature changes (19). Whether SMN deficiency is the direct cause for any of these symptoms is still unproven, and further study is required to define the extent of non-motor neuron involvement in SMA.

A number of mouse models of SMA have been developed. The first models had mouse *Smn* disrupted and contained *SMN2* (20,21), with low copies of *SMN2* leading to SMA and high copy number of *SMN2* rescuing the SMA mice. Subsequently, it has been shown that the transgenic addition of SMN cDNA lacking exon 7 (SMNΔ7, the major gene product of *SMN2*) extends the life span of mice with low *SMN2* copy number and is thus beneficial (22).

We recently demonstrated the efficient transfer of SMN1 in post-natal SMA mice (*SMN2*+/+, SMNΔ7+/+, *Smn*−/−, referred to also as the SMNΔ7 mouse) using self-complementary adeno-associated virus type 9 (scAAV9) (23). SMA mice of this type die at 15 days of age when not treated. Our treated mice survived to well over 200 days of age and showed no signs of motor neuron disease. Another approach using gene delivery with adeno-associated virus vectors in severe SMA mice demonstrated similar findings, yet reported potential cardiac manifestations (24). The treated animals in our study were healthy, but displayed limited necrosis of the eartips which resolved. Other treatments for SMA that extend life to a lesser extent have been reported to result in more widespread necrosis (25). In addition, some milder SMA mice show signs of distal necrosis (21,26). Lastly, some SMA patients are also reported to have decreased blood flow to the extremities leading to discoloration and necrosis, as well as episodes of inappropriate sweating (hyperhydrosis), further implicating dysfunction of the autonomic nervous system (27). One possible explanation for the abnormal blood flow is altered autonomic tone to the cardiovascular system.

The suggestion of altered blood flow in SMA as well as the presence of bradycardia in some SMA patients prompted us to examine whether a cardiac deficit is present in the SMNΔ7 mouse model of SMA and whether any defect found could be corrected by our scAAV9-SMN post-natal gene delivery treatment. Echocardiographic measurements and electrocardiographic (ECG) analysis of the heart revealed that SMA animals are bradycardic and develop a dilated cardiomyopathy (DCM) by 14 days of age, with less severe abnormalities detected as early as 7 days of age. Structural modifications assessed by histological analysis correlated with the *in vivo* functional findings. Remarkably, scAAV9-SMN therapy improved LV remodeling and fully corrected heart rate. Although the mechanisms fully responsible for these cardiac deficits are unknown, neuronal (autonomic) and developmental components may be implicated. Therefore, it is important to investigate whether SMA patients of various severities have or will manifest cardiac deficits.

RESULTS

Echocardiographic analysis of post-natal day 14 SMA mice

Our first step in assessing heart function was to analyze *in vivo* cardiac structure in p14 SMA mice using echocardiography. We studied three groups of animals: healthy wild-type (WT) mice, affected SMA mice and scAAV9-SMN-treated SMA mice. SMA mice have smaller hearts compared with WT, indicated by decreased LV mass (SMA: 27.17 ± 4.46 mg vs. WT: 67.89 ± 1.47 mg, $P < 0.001$; Fig. 1A). We also noted that ventricular walls were significantly thinner in these animals (SMA: 0.34 ± 0.02 mm vs. WT: 0.68 ± 0.03 mm, $P < 0.001$; Fig. 1B). These findings could partially be due to the small size of SMA mice, so we next compared LV wall thickness (posterior wall dimension, PWD) with the LV diameter in diastole (2xPWD/LVDD) in order to normalize and compare LV structure in each group. This ratio is lower in SMA mice (SMA: 0.24 ± 0.01 vs. WT: 0.45 ± 0.03, $P < 0.001$), suggesting eccentric hypertrophy (28) (Fig. 1C). Interestingly, LV mass was increased in p14 scAAV9-SMN-treated animals, compared with SMA mice (AAV9: 42.73 ± 2.451 mg vs. SMA: 27.17 ± 4.460 mg, $P = 0.01$, vs. WT: 67.89 ± 1.47 mg, $P < 0.001$), and both the extent of dilation (2xPWD/LVDD – AAV9: 0.39 ± 0.03 vs. SMA: 0.24 ± 0.01, $P < 0.01$, vs. WT: 0.45 ± 0.03, $P = 0.28$) and wall thinning (AAV9: 0.64 ± 0.03 mm vs. SMA: 0.34 ± 0.02 mm, $P < 0.001$, vs. WT: 0.68 ± 0.03 mm, $P = 0.16$) were attenuated and returned toward WT values.

It is possible that the abnormal heart dimensions represent a slower growth of the heart in proportion to the stunted growth of SMA animals. Therefore, we compared heart weight to body size post-mortem. We used tibia length (TL) as a surrogate measure for body size, since SMA animals experience increased muscular atrophy, thereby making a comparison to body weight invalid. TL in SMA animals are significantly smaller than those of WT animals at both 7 days (WT: 5.15 ± 0.05 mm vs. SMA: 4.87 ± 0.033 mm, $P = 0.016$) and 14 days of age (WT: 10.65 ± 0.35 mm vs. SMA: 7.33 ± 0.17 mm, $P = 0.0023$)

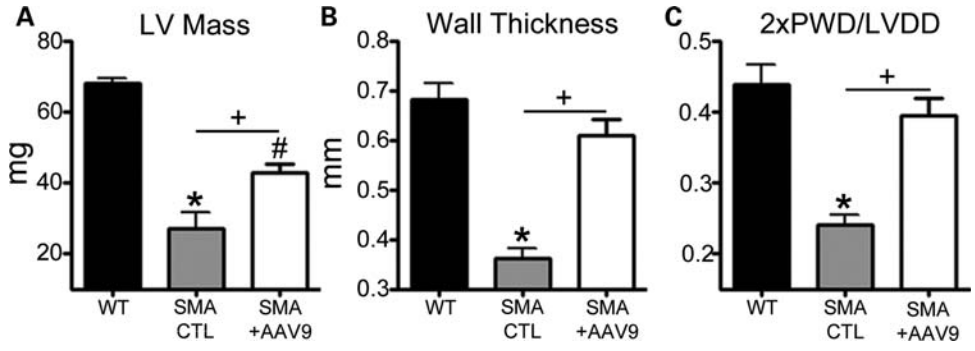

Figure 1. Echocardiographic measurements of (**A**) LV mass, (**B**) wall thickness and (**C**) 2xPWD/LVDD show significant decreases in SMA mice compared with WT and scAAV9-treated animals, suggesting that SMA mice are undergoing eccentric hypertrophy and are at increased risk for heart failure. Although scAAV9-treated mice also have decreased LV mass compared with WT, wall thickness and 2xPWD/LVDD measurements are not significantly changed. Symbols indicate $P < 0.05$ when comparing SMA with WT (*), AAV9 with WT (#) and AAV9 with SMA (+).

(Supplementary Material, Fig. S1A and B). Heart weight to TL ratios (HW:TL) appear slightly decreased in SMA mice of both 7-day-old (WT: 6.29 ± 0.0028 mg/mm vs. SMA: 5.65 ± 0.21 mg/mm, $P = 0.099$) and 14-day-old mice (WT: 4.55 ± 0.75 mg/mm vs. SMA: 3.95 ± 0.032 mg/mm, $P = 0.36$), but these differences were not significant (Supplementary Material, Fig. S1C and D**)**. This implies that the small cardiac mass of SMA mice is correctly proportional to their small body size and that cardiac dilation (2xPWD/LVDD) is not an artifact of an overall reduction in heart mass or stunted growth. We next confirmed that the small size of the SMA animals did not invalidate other cardiac dimensions observed by echocardiography. To do this, we normalized all wall thickness measurements to the average TL for each group. We found that similar differences in wall thickness between SMA and WT animals remain despite normalization to TL in both 7-day-old (WT: 0.094 ± 0.0028 vs. SMA: 0.074 ± 0.0042, $P = 0.0017$) and 14-day-old animals (WT: 0.064 ± 0.0031 vs. SMA: 0.049 ± 0.0028, $P = 0.0086$; Supplementary Material, Fig. S1E and F).

Given that there were significant structural changes occurring in the heart, we next evaluated functional measurements using highly sensitive echocardiography. Echocardiography allows for precise measurements of cardiac function including heart rate, stroke volume (SV), cardiac output, fractional shortening (FS) and Tei index. To perform these studies, we analyzed 5–8 mice in each group using non-invasive measurements with isoflurane gas anesthesia. Anesthesia may affect certain measurements, including heart rate, but given our previous experience in collecting cardiovascular measurements with this protocol along with adequate control mice that were anesthetized, our results are reliable measurements for cardiac function *in vivo*. As expected based on the echocardiographic visualization of the heart, LV function in SMA mice was severely impaired at 14 days of age (Fig. 2). We found that SMA mice presented with a strikingly severe sinus bradycardia, a slowing of heart rate (SMA: 320 ± 19 bpm vs. WT: 452 ± 10 bpm, $P < 0.001$). We next tested SMA mice treated with scAAV9-SMN to determine whether restoring SMN levels could improve the heart rate. Indeed, scAAV9-SMN delivery, which targets neurons within the central and peripheral nervous system as well as the cardiac tissues, completely restored heart rates in treated animals to comparable levels of WT controls (AAV9: 448 ± 11 bpm vs. SMA: 320 ± 19 bpm, $P < 0.001$, vs. WT: 452 ± 10 bpm, $P = 0.97$; Fig. 2A). scAAV9-green fluorescent protein (GFP) delivery had no negative or beneficial cardiac effects on SMA-treated animals for any measurements discussed below (data not shown), and therefore, we analyzed non-injected SMA controls for all remaining studies. SV, the volume of blood pumped with each contraction, was also severely decreased in SMA mice (SMA: 13.08 ± 2.00 μl vs. WT 22.94 ± 5.35 μl, $P = 0.0025$) and delivery of scAAV9-SMN failed to increase levels to that of WT animals (AAV9: 12.85 ± 3.24 μl vs. SMA: 13.08 ± 2.00 μl, $P = 0.891$, vs. WT: 22.94 ± 5.35 μl, $P < 0.01$; Fig. 2B). Cardiac output (heart rate × SV) is significantly decreased in SMA animals (SMA: 4.16 ± 0.30 ml/min vs. WT: 10.29 ± 0.70 ml/min, $P < 0.001$). As expected from the above data, scAAV9-SMN improved, but did not restore, cardiac output compared with WT mice (AAV9: 5.75 ± 0.62 ml/min vs. SMA: 4.16 ± 0.30 ml/min, $P = 0.059$, vs. WT: 10.29 ± 0.70 ml/min, $P < 0.001$), mainly due to the improved heart rate (Fig. 2C). Although the cause of death of SMA mice has been speculated to be due to respiratory failure, animals in our study displayed a high risk for developing a DCM leading to a fatal congestive heart failure as evidenced by the decreased SV and eccentric hypertrophy.

To assess contractility, *m*-mode measurements of the changing ventricular diameter over the cardiac cycle were used to calculate fractional shortening (FS%). We found that SMA mice showed a significant decrease in FS% (SMA: $20.82 \pm 2.05\%$ vs. WT: $39.19 \pm 0.47\%$, $P < 0.001$), consistent with the lower SV already observed. Contractility was increased by scAAV9-SMN treatment, yet it did not completely restore FS to WT levels (AAV9: $27.29 \pm 1.07\%$ vs. SMA: $20.82 \pm 2.05\%$, $P < 0.01$, vs. WT: $39.19 \pm 0.47\%$, $P < 0.001$; Fig. 2D). Additionally, we assessed the LV Tei index, which accounts for the aspects of both systolic and diastolic function [(isovolumic contraction time + isovolumic relaxation time)/aortic ejection time] (29–31). SMA mice, as expected, had a significantly higher LV Tei index than WT (SMA: 0.79 ± 0.09 vs. WT: 0.40 ± 0.02, $P < 0.001$), indicating an overall decrease in function. Treatment with

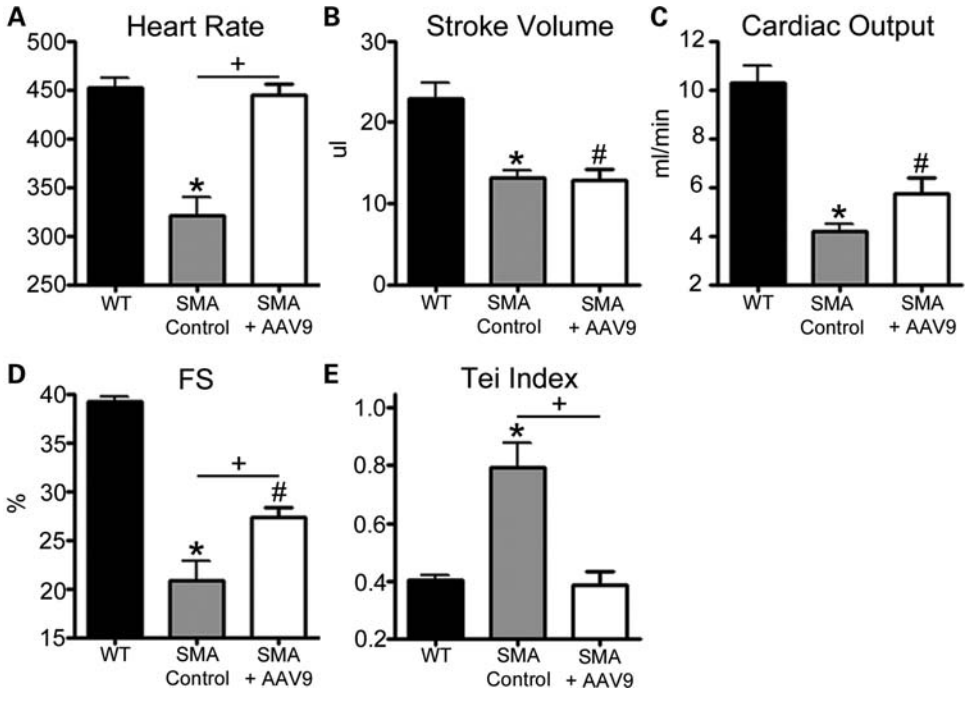

Figure 2. Echocardiographic measurements of cardiac function in p14 mice. Cardiac function of the SMA mice was significantly lower than that of WT mice when we assessed heart rate (**A**), SV (**B**), cardiac output (**C**) and FS (**D**). scAAV9-treated animals have heart rates indistinguishable from WT (A), but SV (B) is similar to SMA animals, thereby decreasing the overall cardiac output as well (C). FS, a measure of contractility, is decreased in both SMA and AAV9 mice, though scAAV9-treated mice contract significantly better than untreated SMA mice (D). Tei index is increased in SMA mice, consistent with worse combined systolic and diastolic function, whereas scAAV9-treated mice have similar values to WT, indicating preserved function (**E**). Symbols indicate $P < 0.05$ when comparing SMA with WT (*), AAV9 with WT (#) and AAV9 with SMA (+).

scAAV9-SMN, however, restored the LV Tei index to levels that were nearly identical to WT mice indicating that gene delivery of SMN post-natally could restore an important measure of cardiac function to normal levels (AAV9: 0.38 ± 0.05 vs. SMA: 0.79 ± 0.09, $P < 0.01$, vs. WT: 0.40 ± 0.02, $P = 0.73$; Fig. 2E).

Echocardiography of p7 animals

Given that we found such dramatic cardiac deficits in structure and function of SMA mice at 14 days of age, we next investigated whether we could detect cardiac abnormalities earlier in the disease (Fig. 3). Indeed, SMA mice at 7 days of age presented with early anatomical differences in both LV and right ventricle compared with WT animals. LV mass was decreased significantly in SMA mice (SMA: 17.94 ± 2.03 mg vs. WT: 33.50 ± 1.03 mg, $P < 0.001$) and treatment with scAAV9-SMN in post-natal day 1 mice led to an increase in mass, yet did not restore mass to WT levels (AAV9: 23.36 ± 1.65 mg vs. SMA: 17.94 ± 2.03 mg, $P = 0.077$, vs. WT: 33.50 ± 1.03 mg, $P < 0.001$; Fig. 3A). Wall thickness was significantly decreased in SMA mice (SMA: 0.36 ± 0.02 mm vs. WT: 0.47 ± 0.02 mm, $P < 0.01$), yet scAAV9-SMN delivery completely preserved wall thickness in treated animals to similar levels as WT controls (AAV9: 0.43 ± 0.02 mm vs. WT: 0.47 ± 0.02 mm, $P = 0.15$; Fig. 3B). We next used the same measure of eccentric dilation as described above (2xPWD/LVDD) and found that the ratio was smaller in SMA mice (SMA: 0.30 ± 0.02 vs. WT: 0.40 ± 0.02, $P < 0.01$), yet was partially corrected in scAAV9-treated mice to levels similar to WT controls (AAV9: 0.35 ± 0.02 vs. SMA: 0.30 ± 0.02, $P = 0.078$, vs. WT: 0.40 ± 0.02, $P = 0.09$; Fig. 3C).

In the course of our functional measurements, the most striking cardiac finding in post-natal day 7 SMA animals was significantly lower heart rates compared with WT animals (SMA: 354 ± 18 bpm vs. WT: 444 ± 15 bpm, $P < 0.001$). Similar to post-natal day 14 animals, delivery of scAAV9-SMN at 1 day of age increased heart rates to levels similar to controls (AAV9: 439 ± 18 bpm vs. SMA: 354 ± 18 bpm, $P < 0.01$, vs. WT: 444 ± 15 bpm, $P = 0.83$; Fig. 3D). We found as early as 7 days of age that SMA mice had a significant decrease in FS (SMA: $17.20 \pm 2.23\%$ vs. WT: $37.3 \pm 0.29\%$, $P < 0.001$) as assessed by *m*-mode echocardiography. Delivery of scAAV9-SMN significantly increased this measure of contractility. However, scAAV9-treated mice still had much lower FS compared with WT (AAV9: $25.84 \pm 1.6\%$ vs. SMA: $17.20 \pm 2.23\%$ $P < 0.01$, vs. WT: $37.3 \pm 0.29\%$, $P < 0.001$; Fig. 3E). Tei index in SMA mice was increased at this early time point (SMA: 0.54 ± 0.04 vs. WT: 0.33 ± 0.02, $P < 0.01$); however, this increase was smaller than that seen in 14-day-old animals (i.e. a difference between SMA and WT of 0.22 in 7-day olds vs. 0.39 in 14-day olds), suggesting a gradual progression of heart failure. Tei index was partially preserved in scAAV9-treated mice at 7 days of age, demonstrating an early effect of scAAV9-SMN treatment (AAV9: 0.44 ± 0.04 vs. SMA: 0.54 ± 0.04, $P = 0.119$, vs. WT: 0.33 ± 0.02, $P < 0.05$; Fig. 3F).

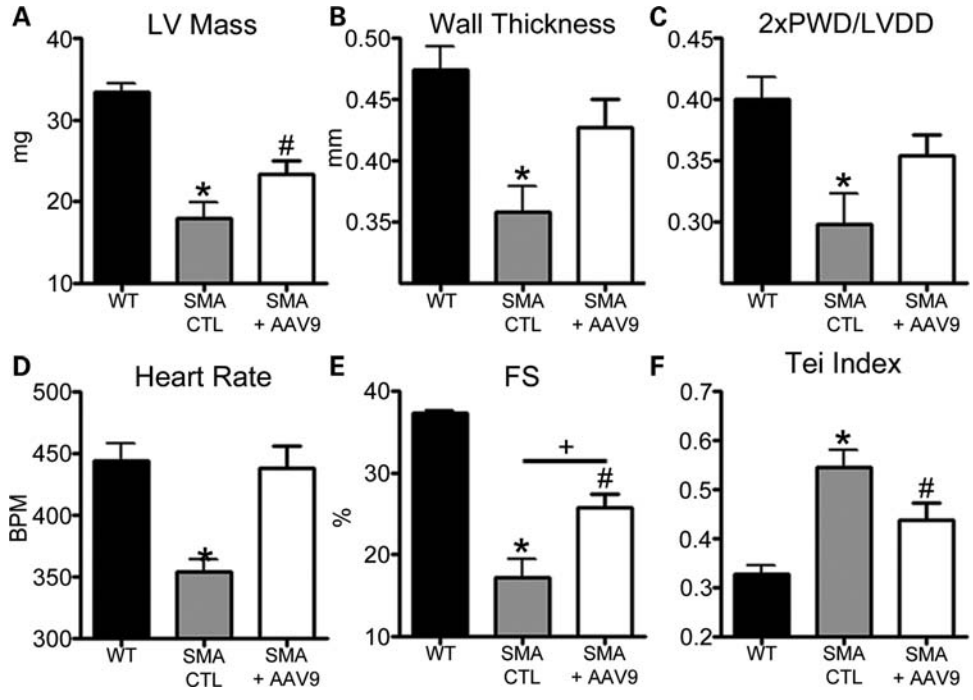

Figure 3. Echocardiographic measurements of cardiac function in p7 mice. As with p14 animals, measures of LV mass (**A**), wall thickness (**B**), dilation (**C**), heart rate (**D**), FS (**E**) and Tei index (**F**) all indicate decreased function in SMA mice, whereas functional measures in scAAV9-treated animals are relatively preserved. Symbols indicate $P < 0.05$ when comparing SMA with WT (*), AAV9 with WT (#) and AAV9 with SMA (+).

Histopathological analysis of p14 and p7 animals

We next evaluated the hearts by histological analysis to determine the pathological nature of the cardiac deficits occurring early in SMA mice. Gross analysis of the heart confirmed the echocardiographic findings of dilated ventricles and thinning walls on both p7 and p14 SMA mice. Pathological analysis of sections from the hearts of SMA mice using hematoxylin and eosin (H&E) staining showed no signs of inflammation, ischemia or cellular disorder (Fig. 4A–D). We next performed stains to determine if there was early damage leading to collagen deposition in the heart. Indeed, in models of eccentric dilation, a change in the percentage of collagen volume has been observed and is used as an additional marker for cardiac tissue damage. To assess our SMA mice, we quantified the amount of collagen present in SMA hearts. We found no increase in collagen in 14-day-old SMA mice compared with WT animals using Mason's trichrome and picrosirius red (PSR) stains, indicating no fibrosis occurring at these time points.

Although there were significant cardiac functional deficits with no associated pathological abnormalities of cardiomyocytes based on histological evaluation, we next wished to analyze cardiomyocytes of SMA animals by transmission electron microscopy (TEM) in order to further examine the ultrastructure of cardiomyocytes. Analysis of SMA hearts surprisingly revealed significant ultrastructural changes in cardiomyocytes (Fig. 4E and F). In 14-day-old SMA cardiomyocytes, mitochondria were found to be swollen in size. In some instances, the myocyte sarcoplasm was nearly filled with mitochondria. Numerous mitochondria also showed degenerative changes such as the fragmentation of cristae along with associated vacuolar degeneration (Fig. 4F, inset). There was marked disorganization and degeneration of myofibers with focal areas of vacuolar change and generalized loss of sarcomeric detail, where only Z-lines remain clearly defined (Fig. 4F, asterisk). The presence of myelin bodies throughout the tissue indicates increased organelle and/or membrane turnover, implying significant cardiac dysfunction. We also found that cardiac myocyte diameter was similar between SMA and WT mice at 14 days (WT: 9.63 ± 0.38 μm vs. SMA: 11.83 ± 1.50 μm, $P = 0.34$; Supplementary Material, Fig. S2), which is contrary to what is seen in skeletal muscle of SMA mouse models and patients. In fact, there was a slight increase in cardiomyocyte diameter that could be due to the changes noted by TEM of swollen myofibers and mitochondria, although this increase was not statistically significant.

Dobutamine stress challenge

In order to determine whether the functional and ultrastructural changes were due to decreased sensitivity of the heart to autonomic stimulation, we next recorded our animals' responses to dobutamine (Fig. 5). Dobutamine is a sympathomimetic which should increase both heart rate and contractility in hearts that express the correct complement of adrenergic receptors. As expected, both WT and SMA animals responded appropriately by increasing heart rate 4 min after dobutamine injection (percent increase over baseline heart rate—SMA: $24.93 \pm 4.92\%$ vs. WT: $27.87 \pm 6.18\%$, $P = 0.717$; Fig. 5A). Similarly, contractility (as indicated by FS%) increased significantly in WT and SMA groups after injection, though SMA animals responded to a

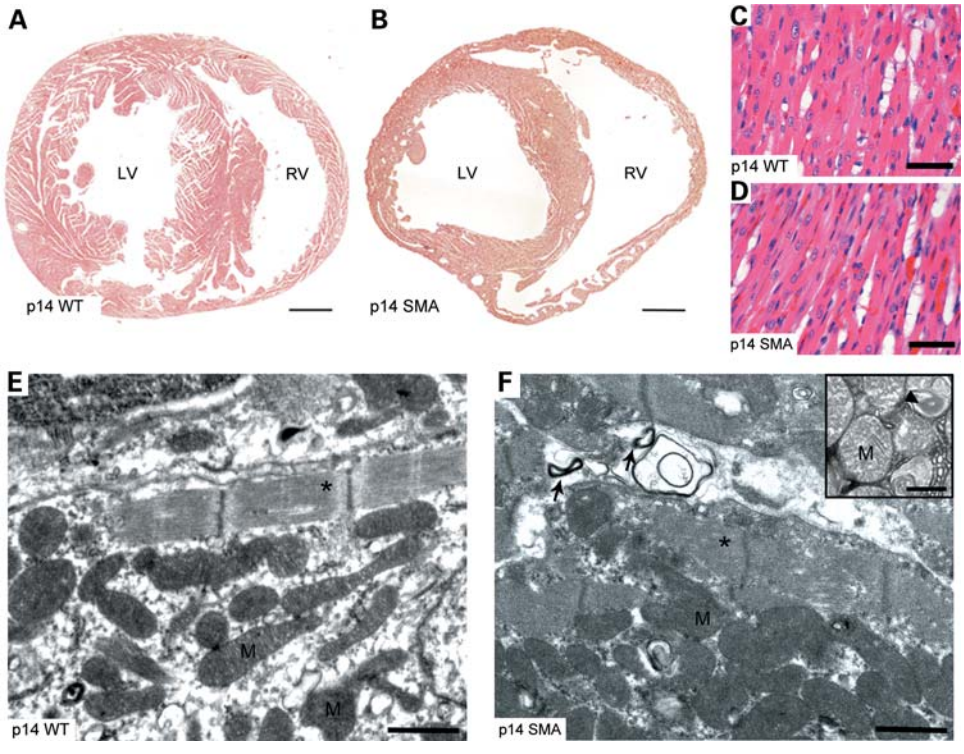

Figure 4. Cardiac histology of p14 mice. H&E mid-ventricular sections show the typical thinning heart walls and dilated ventricles of SMA mice (**B**) compared with WT (**A**) (tiled images, scale = 500 μm). Higher-power images (×40 magnification, scale = 30 μm) of WT (**C**) and SMA mice (**D**) both show absence of inflammation or other signs of overt tissue pathology at p14. TEM of WT mice (**E**) show normal mitochondria (M) and myofibers with well-organized fibrils and well-defined sarcomeres (asterisk, Z-line) (scale = 1 μm). TEM sections of SMA heart tissue (**F**) show swollen myofibers with disorganized Z-lines (asterisk) and no clearly defined I bands, A bands or H zones (scale = 1 μm). Mitochondria in SMA myocytes are swollen with evidence of crystolysis (mitochondria marked by 'M'), and in many fields, these organelles occupy most of the sarcoplasm. The inset (F) shows a clearer view of degenerating mitochondria with myelin figure formation (evidence of advanced crystolysis and membrane degradation) (arrowhead) (scale = 0.5 μm).

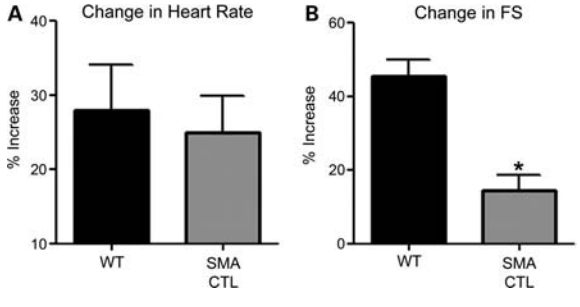

Figure 5. Dobutamine stress challenge in p14 WT and SMA mice. Heart rate, as expected, increases upon dobutamine administration in WT and SMA mice (**A**). FS also increases upon dobutamine administration in both groups, whereas in SMA mice, FS increases to a significantly lesser degree (**B**). In B, asterisk denotes significance ($P < 0.05$) compared with WT.

lower degree (percent increase over baseline FS%—SMA: 14.58 ± 4.16% vs. WT: 45.36 ± 4.59%, $P < 0.001$; Fig. 5B**)**, likely due to decreased contractile reserve, which is common in heart failure (32).

Autonomic targets of scAAV9

The autonomic nervous system helps to maintain blood pressure in part by altering pacemaker activity and signal conduction in the heart (Fig. 6A). The paraventricular nucleus (PVN) of the hypothalamus primarily sets the tone of the sympathetic nervous system by positively stimulating neurons in the nucleus of the tractus solitarius (NTS). NTS neurons integrate input from the PVN and peripheral baroreceptors and send stimulatory projections to the intermediolateral column of the spinal cord (IML), which project to the paravertebral sympathetic ganglia (SG) and on to the heart, stimulating increased heart rate and contractility through the activation of noradrenergic receptors. The vagal nuclei [motor nucleus of the vagal nerve (MNX) and nucleus ambiguus (NA)] are primarily responsible for decreasing heart rate. Vagal fibers project to the cardiac ganglia (CG), which then decreases heart rate primarily by slowing nodal conduction.

Owing to the remarkable rescue of the heart rate in scAAV9-treated animals, we sought to determine which neurological structures relating to cardiac pacing were transduced following scAAV9-SMN administration. To do this, we injected neonatal WT animals with scAAV9 carrying a GFP transgene to visualize which tissues were transduced (33). We visualized all the nuclei and ganglia mentioned above, and high-power images of these autonomic loci are shown in Figure 6B–I. Of these structures, the MNX, NA, CG and the SG are highly transduced and quantification of these autonomic nuclei using sections of brain, spinal cord and heart revealed 90, 100, 60 and 50% transduction, respectively), whereas the PVN, NTS and IML revealed no

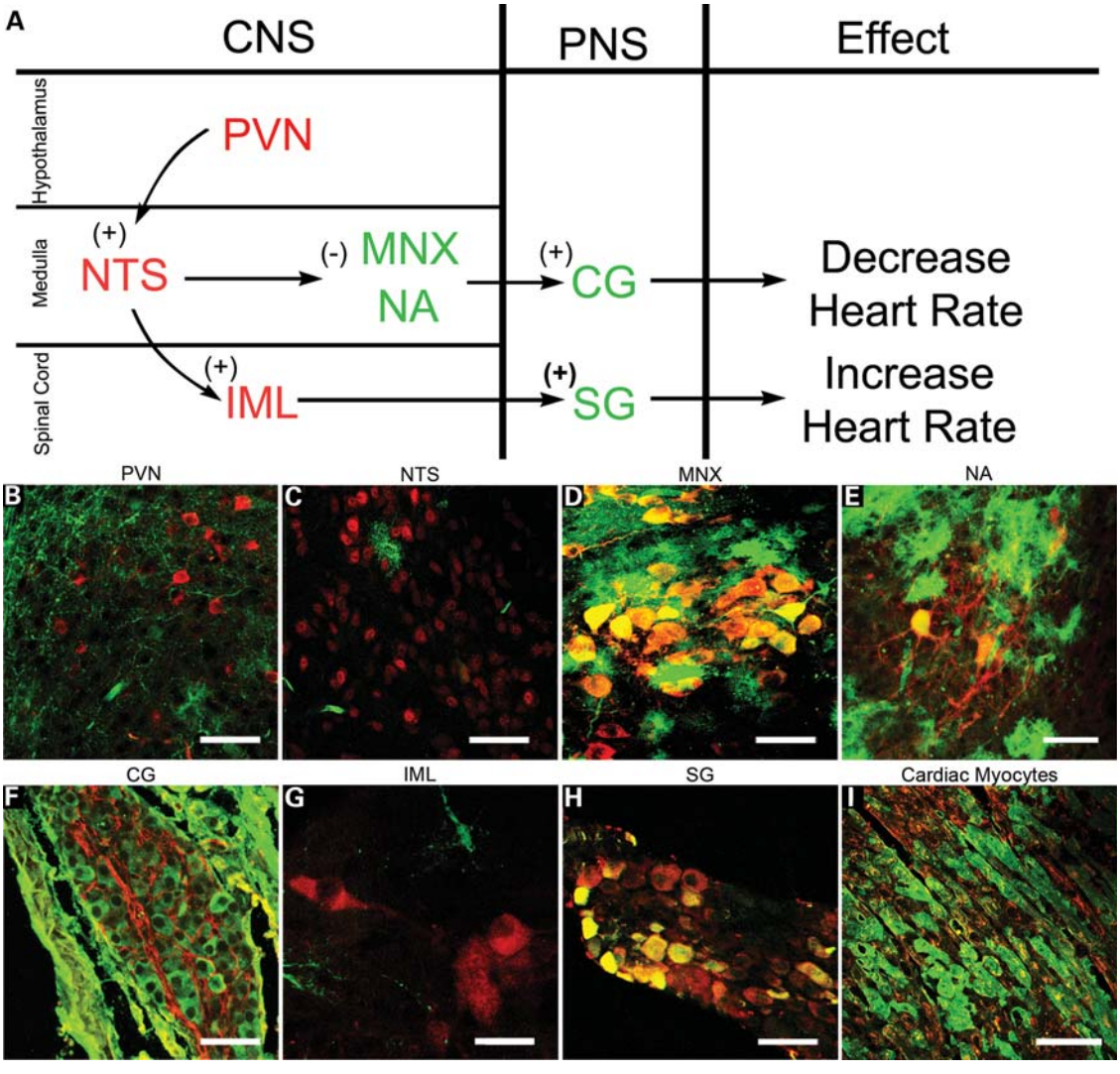

Figure 6. A schematic overview of the key neuronal structures controlling heart rate (**A**). The sympathetic structures observed were the PVN, the NTS, the IML and the SG. The parasympathetic structures observed include the MNX, the NA, the NTS and the CG. scAAV9 transduction can be assessed by visualizing the presence of a green fluorescent protein (GFP) transgene (**B**–**I**). The MNX (D), NA (E), CG (F) and SG (H) were all highly transduced, whereas we found no evidence of transduction of the PVN (B), NTS (C) and IML (G) neurons. Cardiac myocytes were also found to be mostly positive for the GFP transgene (I). Green, GFP in B–I; Red, tyrosine hydroxylase in B and H, neuronal nuclei (NeuN) in C, choline acetyl-transferase (ChAT) in D, E and G, neurofilament-160 (NF-160) in F and dystrophin in I. Scale = 50μm in B–F, H and I, and 20 μm in G.

significant transgene expression. Besides these neuronal targets, cardiac myocytes of the ventricles and atria are also very well transduced (over 80%), which has been reported previously (34,35) demonstrating that vascularly delivered scAAV9 can target most of the cardiac tissues as well as the innervating autonomic nervous system that assists in the regulation of cardiac function.

DISCUSSION

Although the number of case reports presenting cardiac abnormalities in SMA patients is increasing, there have been few to no highly powered and controlled studies regarding cardiovascular anomalies in SMA. Despite the existence of mouse models for SMA, to date there have been no reports of cardiac dysfunction in these animals. In this study, we specifically evaluated the potential for cardiac manifestation in a severe model of SMA that is routinely used for drug- and therapeutic-based screening. In this new report, we have shown that SMN deficiency leads to early and persistent cardiac dysfunction in mice.

SMA mice display many symptoms of cardiac involvement consistent with what is found in the limited reports on human SMA patients. These similarities include a notable bradycardia similar to what has been reported in over 20% of type 1 SMA patients (17,18). Interestingly, our results using light and electron microscopy are consistent with an early analysis of an endomyocardial biopsy from a type 3 SMA patient (36). We found that myocytes in SMA mice have disorganized myofibers, swollen, disorganized mitochondria and evidence of organelle and/or membrane turnover. In the mouse, we found that >90% of myocytes exhibited ultrastructural

pathology, where only 2–4% of myocytes in the reported type 3 SMA patient demonstrated pathology. This is not surprising, though, given that the SMNΔ7 animal models a significantly more severe disease than what is seen in type 3 SMA patients. To our knowledge, no studies have evaluated cardiac ultrastructural pathology in type 1 SMA patients. The exact cause of mitochondrial swelling seen in SMA mice or its relationship to *Smn* deficiency is unknown; however, mitochondrial swelling has been reported in ischemia/reperfusion cardiac injury due to potential increased energy demand on the heart (37). The increased size of mitochondria in the failing SMA myocardium therefore may be explained as a result of compensatory mechanisms due to increased energy demand. This may also be due to a maladaptive response leading to the release of oxidative cytochromes, and/or the onset of mitochondrial permeability transition, both of which are detrimental to cardiac pump function (38).

Contrary to human case reports, we did not observe any septal defects using echocardiography. This is not surprising as these defects were only reported in very severe type 0 SMA patients (18), and the SMA mice used in this study are thought to model a more moderate phenotype (i.e. type 1 or 2 SMA) (22). In contrast to the overt, progressive development of DCM in all SMA mice examined in this study, there are few reports of human SMA patients developing DCM (16,39), and this is mostly reported in patients with less severe forms of SMA. However, this may due to the fact that most type 1 patients die before thorough cardiac evaluation and should be a subject of future study.

Heart rate is regulated by neuronal, hormonal and local mechanisms within the heart. Possible reasons for bradycardia include increased vagal (parasympathetic) tone, decreased sympathetic tone and/or alteration of the nodal and conduction systems in the heart itself. The limited response to the dobutamine stress challenge is typical of heart failure patients (40), but it demonstrates that the hearts of SMA mice can, at least partially, respond to sympathetic stimulation by increasing heart rate. This evidence, together with the fact that scAAV9-SMN is able to transduce 4 out of 7 key autonomic loci and rescue the heart rate deficit leads us to believe that autonomic dysfunction may be the primary cause of bradycardia in SMA mice.

Correct regulation of heart rate is extremely important—not only to ensure proper perfusion throughout the body, but also to protect the heart against undue stress. Neonatal bradycardia has been linked to DCM in experimental rodents (41) and in human patients (42,43). It is not surprising, then, that SMA mice develop a very early DCM, especially since we observed slower heart rates in affected animals as early as 3 days after birth (data not shown). Furthermore, hearts with DCM are more susceptible to increased wall stress, leading to decreased function and remodeling of heart tissue. Progressive remodeling can cause development of both systolic and diastolic dysfunction, consistent with an increased Tei index as seen in our p7 and p14 animals. Independent of neuromuscular function, SMA mice are at high risk for early congestive heart failure which has been under-appreciated as a potential confounding factor in therapeutic studies to date.

It appears that the success of scAAV9-SMN treatment is not solely determined by its ability to transduce spinal motor neurons, but also its ability to target the autonomic nervous system. Early post-natal delivery of scAAV9-SMN was able to treat bradycardia and prevent the early development of DCM. Despite the highly successful rescue of heart rate, the relatively normal wall dimensions and efficient transduction of cardiomyocytes, the hearts of treated animals show decreased contractility compared with WT hearts. These results suggest that additional mechanisms also contribute to SMA-associated contractile dysfunction. We cannot rule out the possibility that myocyte stress is inflicted *in utero* by autonomic dysfunction prior to treatment with scAAV9-SMN or that SMN plays a key role in cardiac development that we are unable to treat post-natally. SMA mice can also be malnourished, and anorexia is already a known cause of cardiac dysfunction (44). Furthermore, the disordered metabolic state caused by muscular atrophy and respiratory distress further complicate the identification of the mechanisms contributing to SMA-associated contractile dysfunction. Future studies should investigate these potential factors. Additionally, it should be determined whether the deficits are unique to the mouse, and correlation between disease severity and extent of cardiac involvement should be assessed.

As the overall lifespan of SMA patients has increased over the past decade and as new drugs and therapies that extend survival of SMA patients emerge, clinicians should be acutely aware of potential heart dysfunction in a subset of SMA patients. SMA patients already have compromised lung function, so potential causes of any additional pulmonary complication (i.e. from congestive heart failure) should be anticipated and closely monitored. Additionally, SMA patients are commonly intubated for respiratory support and can become autonomically unstable due to vagal irritation. The fragility of these patients and the increasing reports of autonomic dysfunction together with our current findings warrant increased attention to the cardiac status of SMA patients, and it potentially highlights the need to investigate cardiac interventions alongside neuromuscular treatments.

MATERIALS AND METHODS

AAV9 injection of neonatal mice

Animals were injected as described previously (23,33) with 5×10^{11} particles of scAAV9-SMN or scAAV9-GFP.

Anesthetic protocol

Anesthesia was induced by placing 7- and 14-day mouse neonates in an induction chamber supplied with 4% isoflurane anesthesia delivered in 100% oxygen at a flow rate of 1 l/min. Sedated mice were transferred to a heated pad set to maintain body temperature at 37°C, and paws were placed on ECG leads. A nosecone was placed over the nose and 2% isoflurane was administered in 100% oxygen at a flow rate of 1 l/min. Excess gases were removed using a vacuum scavenging system.

Echocardiographic analysis

A Visual Sonics 2100 Ultra High Resolution *In Vivo* Imaging System (VisualSonics, Toronto, ON, Canada) was used to

perform echocardiographic studies. Three measures at different cardiac cycles were used for analysis according to the standards set forth by the American Society for Echocardiography leading edge method. Examples of how images were analyzed are included in Supplementary Material, Figure S3. Each individual was analyzed in ~20 min. A scan head with a center frequency of 40 MHz and lateral resolution of 80 μM was used for all measurements. Prewarmed ultrasound transmission gel (Aquasonic, Parker Laboratory, Fairfield, NJ, USA) was placed on the scan head. Two-dimensional long-axis images were visualized in the left parasternal position in order to measure the LV outflow tract and calculate the LV mass:

$$\begin{aligned}\text{LV mass (mg)} = & 1.05 \times \{[5/6 \times \text{Epicardial area}; \\ & d \times (\text{Epicardial major}; d + T)] \\ & - [5/6 \times \text{Epicardial area}; \\ & d \times (\text{Epicardialminor}; d + T)]\}\end{aligned}$$

To determine LV SV, color Doppler was used as an overlay to determine the point of fastest flow in the aorta. Pulse Doppler echocardiographic analysis with a sampling size of 0.6 mm was used to measure the flow at this point and the velocity time interval (VTI) was obtained. SV was calculated using the following formula:

$$\text{SV}\,(\mu\text{l}) = 7.85 \times \text{LVOT}^2 \times \text{Ao VTI}$$

Cardiac output was calculated from the measurement of SV:

$$\text{CO}\,(\text{ml}/\,\text{min}) = (\text{SV} \times \text{HR})$$

From the four-chamber view, pulse Doppler images were obtained with the sample volume placed just to the left of center of the mitral orifice and at the tips of the mitral leaflets. At this point, we obtained images with both the mitral inflow and the LV outflow providing us with the isovolumetric relaxation (IVRT), isovolumetric contraction (IVCT) and aortic ejection time (ET). Using these values, we calculated the Tei index:

$$\text{Tei} = \frac{\text{IVRT} + \text{IVCT}}{\text{ET}}$$

M-mode images were obtained at the level of the papillary muscles in order to assess LV end-diastolic diameter (LVEDD), LV end-systolic diameter (LVESD) and LV wall thicknesses. Eccentric hypertrophy was calculated as 2 × PWD/LVEDD. Systolic function was assessed using *m*-mode calculations of FS:

$$\text{FS} = \frac{\text{LVEDD} - \text{LVESD}}{\text{LVEDD}} \times 100$$

Dobutamine stress echocardiography

After baseline images were acquired, 0.5 mg/kg of dobutamine was injected intraperitoneally. Heart rate was monitored until a stable peak was reached after ~4 min. *M*-mode images were acquired at the level of the papillary muscles and FS was calculated.

Mouse breeding and genotyping

All breeding and subsequent use of animals in this study were approved by the IACUCs of the Research Institute at Nationwide Children's Hospital in and/or the Ohio State University Columbus, OH, USA0. The genotype of all breeding pairs used is human *SMN*2+/+, human SMNΔ7+/+ and mouse *Smn*+/−. Upon the discovery of new birth, all newborn mice were briefly removed from their mother's cage, tattooed for identification and a small piece of tail was taken for genotype analysis. Genomic DNA was extracted and added to two different PCR for the mouse *Smn* allele (forward 1: 5′-TC CAGCTCCGGGATATTGGGATTG, reverse 1: 5′-AGGTCC CACCACCTAAGAAAGCC; forward 2: 5′-GTGTCTGGGC TGTAGGCATTGC, reverse 2: 5′-GCTGTGCCTTTTGGCT TATCTG) and one reaction for the mouse *Smn* knockout allele (forward: 5′-GCCTGCGATGTCGGTTTCTGTGAGG, reverse: 5′-CCAGCGCGGATCGGTCAGACG).

Euthanasia and tissue collection

Each animal was given a lethal dose of ketamine/xylazine anesthetic cocktail via i.p. injection. Intracardiac perfusion with normal saline followed by ice-cold 4% buffered paraformaldehyde (PFA) solution containing 60 mM KCl to arrest heart in diastole. All tissues were then removed and post-fixed at least 24 h in PFA.

Heart histology

Prior to embedding, the base and the apex of each heart were dissected from the mid-ventricular portion. Tissues were moved to 70% ethanol for at least 24 h, then embedded in paraffin. Four micrometer histological sections were taken and stained using H&E, Mason's trichrome and PSR reagents.

Post-mortem heart and tibia recovery

After mice were euthanized in a CO_2 chamber according to the institutional and the AAALAC guidelines, we removed the heart and tibia by gross dissection from the body. Weights were taken after the hearts were cleaned of pluck, chambers were emptied of blood, and tibias were cleaned of extraneous tissues.

Electron microscopy

Hearts collected immediately after euthanasia were fixed in 2.5% glutaraldehyde for a minimum of 24 h and post-fixed in 2% osmium tetroxide in 0.1 M cacodylate buffer. Tissue was rapidly dehydrated in increasing concentrations of ethanol (30–100%), infiltrated with 100% acetone and embedded in low-viscosity polymerized epoxy resin (Spurr's). Sections of 1200 Å length were stained on grids with 1% uranyl acetate and lead citrate. Electron micrographs

were taken with an FEI Technei transmission electron microscope.

Immunohistochemistry

Brains and spinal cords were cut to 40 μm thick and stained as floating sections. Tissues were blocked in 10% donkey serum and 0.1–1% Triton X-100 in TBS solution for 1 h. Tissues were then incubated at 4°C for 24–48 h in diluted primary antibodies in blocking solution. Primary antibodies used: rabbit anti-GFP, 1:400 (Invitrogen); Mouse anti-TH, 1:500 (Sigma-Aldrich); Mouse anti-NeuN, 1:100 (Millipore); Goat-anti-ChAT, 1:200 (Chemicon); Mouse anti-neurofilament 160, 1:500 (Chemicon); Chicken anti-GFP, 1:400 (Abcam); Mouse anti-Dystrophin (Developmental Studies Hybridoma Bank, University of Iowa). After washing, tissues were incubated for 2 h at room-temperature in FITC- or Cy3-conjugated secondary antibodies diluted 1:200 (Jackson ImmunoResearch) and mounted with PVA-DABCO.

Data analysis

Data were analyzed using Prism statistical software (Graphpad). All results are expressed as the mean ± SEM. Differences between groups were considered statistically significant at $P < 0.05$. A one-way ANOVA was used to compare echocardiography data between WT, SMA and scAAV9-treated groups. All echocardiographic parameters were assessed three times at different points of the cardiac cycle.

SUPPLEMENTARY MATERIAL

Supplementary Material is available at *HMG* online.

ACKNOWLEDGEMENTS

We would like to give special thanks to Dr Chicoine and Terri Shaffer and the Small Animal Imaging Facility (SAIF) at the Research Institute at Nationwide Children's Hospital for use of the Visual Sonics 2100 Ultra High Resolution *In Vivo* Imaging System.

Conflict of Interest statement. None declared.

FUNDING

This work was supported by the National Institutes of Health (R21-NS064328 to B.K.K.; R01-NS038650 to A.H.M.B.; RC2-NS069476 to B.K.K. and A.H.M.B.; 2R01-HL5604-12 to P.A.L.) and Miracle for Madison to B.K.K. and A.H.M.B.

REFERENCES

1. Roberts, D.F., Chavez, J. and Court, S.D. (1970) The genetic component in child mortality. *Arch. Dis. Child.*, **45**, 33–38.
2. Lefebvre, S., Burglen, L., Reboullet, S., Clermont, O., Burlet, P., Viollet, L., Benichou, B., Cruaud, C., Millasseau, P., Zeviani, M. *et al.* (1995) Identification and characterization of a spinal muscular atrophy-determining gene. *Cell*, **80**, 155–165.
3. Burghes, A.H. and Beattie, C.E. (2009) Spinal muscular atrophy: why do low levels of survival motor neuron protein make motor neurons sick? *Nat. Rev. Neurosci.*, **10**, 597–609.
4. Lefebvre, S., Burlet, P., Liu, Q., Bertrandy, S., Clermont, O., Munnich, A., Dreyfuss, G. and Melki, J. (1997) Correlation between severity and SMN protein level in spinal muscular atrophy. *Nat. Genet.*, **16**, 265–269.
5. Coovert, D.D., Le, T.T., McAndrew, P.E., Strasswimmer, J., Crawford, T.O., Mendell, J.R., Coulson, S.E., Androphy, E.J., Prior, T.W. and Burghes, A.H. (1997) The survival motor neuron protein in spinal muscular atrophy. *Hum. Mol. Genet.*, **6**, 1205–1214.
6. Lorson, C.L., Hahnen, E., Androphy, E.J. and Wirth, B. (1999) A single nucleotide in the SMN gene regulates splicing and is responsible for spinal muscular atrophy. *Proc. Natl Acad. Sci. USA*, **96**, 6307–6311.
7. Monani, U.R., Lorson, C.L., Parsons, D.W., Prior, T.W., Androphy, E.J., Burghes, A.H. and McPherson, J.D. (1999) A single nucleotide difference that alters splicing patterns distinguishes the SMA gene SMN1 from the copy gene SMN2. *Hum. Mol. Genet.*, **8**, 1177–1183.
8. Cartegni, L. and Krainer, A.R. (2002) Disruption of an SF2/ASF-dependent exonic splicing enhancer in SMN2 causes spinal muscular atrophy in the absence of SMN1. *Nat. Genet.*, **30**, 377–384.
9. Kashima, T. and Manley, J.L. (2003) A negative element in SMN2 exon 7 inhibits splicing in spinal muscular atrophy. *Nat. Genet.*, **34**, 460–463.
10. Gennarelli, M., Lucarelli, M., Capon, F., Pizzuti, A., Merlini, L., Angelini, C., Novelli, G. and Dallapiccola, B. (1995) Survival motor neuron gene transcript analysis in muscles from spinal muscular atrophy patients. *Biochem. Biophys. Res. Commun.*, **213**, 342–348.
11. Lorson, C.L., Strasswimmer, J., Yao, J.M., Baleja, J.D., Hahnen, E., Wirth, B., Le, T., Burghes, A.H. and Androphy, E.J. (1998) SMN oligomerization defect correlates with spinal muscular atrophy severity. *Nat. Genet.*, **19**, 63–66.
12. Lorson, C.L. and Androphy, E.J. (2000) An exonic enhancer is required for inclusion of an essential exon in the SMA-determining gene SMN. *Hum. Mol. Genet.*, **9**, 259–265.
13. Burnett, B.G., Munoz, E., Tandon, A., Kwon, D.Y., Sumner, C.J. and Fischbeck, K.H. (2009) Regulation of SMN protein stability. *Mol. Cell. Biol.*, **29**, 1107–1115.
14. McAndrew, P.E., Parsons, D.W., Simard, L.R., Rochette, C., Ray, P.N., Mendell, J.R., Prior, T.W. and Burghes, A.H. (1997) Identification of proximal spinal muscular atrophy carriers and patients by analysis of SMNT and SMNC gene copy number. *Am. J. Hum. Genet.*, **60**, 1411–1422.
15. Mailman, M.D., Heinz, J.W., Papp, A.C., Snyder, P.J., Sedra, M.S., Wirth, B., Burghes, A.H. and Prior, T.W. (2002) Molecular analysis of spinal muscular atrophy and modification of the phenotype by SMN2. *Genet. Med.*, **4**, 20–26.
16. Finsterer, J. and Stollberger, C. (1999) Cardiac involvement in Werdnig–Hoffmann's spinal muscular atrophy. *Cardiology*, **92**, 178–182.
17. Bach, J.R. (2007) Medical considerations of long-term survival of Werdnig–Hoffmann disease. *Am. J. Phys. Med. Rehabil.*, **86**, 349–355.
18. Rudnik-Schoneborn, S., Heller, R., Berg, C., Betzler, C., Grimm, T., Eggermann, T., Eggermann, K., Wirth, R., Wirth, B. and Zerres, K. (2008) Congenital heart disease is a feature of severe infantile spinal muscular atrophy. *J. Med. Genet.*, **45**, 635–638.
19. Hachiya, Y., Arai, H., Hayashi, M., Kumada, S., Furushima, W., Ohtsuka, E., Ito, Y., Uchiyama, A. and Kurata, K. (2005) Autonomic dysfunction in cases of spinal muscular atrophy type 1 with long survival. *Brain Dev.*, **27**, 574–578.
20. Monani, U.R., Sendtner, M., Coovert, D.D., Parsons, D.W., Andreassi, C., Le, T.T., Jablonka, S., Schrank, B., Rossoll, W., Prior, T.W. *et al.* (2000) The human centromeric survival motor neuron gene (SMN2) rescues embryonic lethality in Smn(-/-) mice and results in a mouse with spinal muscular atrophy. *Hum. Mol. Genet.*, **9**, 333–339.
21. Hsieh-Li, H.M., Chang, J.G., Jong, Y.J., Wu, M.H., Wang, N.M., Tsai, C.H. and Li, H. (2000) A mouse model for spinal muscular atrophy. *Nat. Genet.*, **24**, 66–70.
22. Le, T.T., Pham, L.T., Butchbach, M.E., Zhang, H.L., Monani, U.R., Coovert, D.D., Gavrilina, T.O., Xing, L., Bassell, G.J. and Burghes, A.H. (2005) SMNDelta7, the major product of the centromeric survival motor neuron (SMN2) gene, extends survival in mice with spinal muscular atrophy and associates with full-length SMN. *Hum. Mol. Genet.*, **14**, 845–857.
23. Foust, K.D., Wang, X., McGovern, V.L., Braun, L., Bevan, A.K., Haidet, A.M., Le, T.T., Morales, P.R., Rich, M.M., Burghes, A.H. *et al.* (2010)

Rescue of the spinal muscular atrophy phenotype in a mouse model by early postnatal delivery of SMN. *Nat. Biotechnol.*, **28**, 271–274.
24. Passini, M.A., Bu, J., Roskelley, E.M., Richards, A.M., Sardi, S.P., O'Riordan, C.R., Klinger, K.W., Shihabuddin, L.S. and Cheng, S.H. (2010) CNS-targeted gene therapy improves survival and motor function in a mouse model of spinal muscular atrophy. *J. Clin. Invest.*, **120**, 1253–1264.
25. Narver, H.L., Kong, L., Burnett, B.G., Choe, D.W., Bosch-Marce, M., Taye, A.A., Eckhaus, M.A. and Sumner, C.J. (2008) Sustained improvement of spinal muscular atrophy mice treated with trichostatin A plus nutrition. *Ann. Neurol.*, **64**, 465–470.
26. Gavrilina, T.O., McGovern, V.L., Workman, E., Crawford, T.O., Gogliotti, R.G., DiDonato, C.J., Monani, U.R., Morris, G.E. and Burghes, A.H. (2008) Neuronal SMN expression corrects spinal muscular atrophy in severe SMA mice while muscle-specific SMN expression has no phenotypic effect. *Hum. Mol. Genet.*, **17**, 1063–1075.
27. Araujo Ade, Q., Araujo, M. and Swoboda, K.J. (2009) Vascular perfusion abnormalities in infants with spinal muscular atrophy. *J. Pediatr.*, **155**, 292–294.
28. Shenouda, S.K., Lord, K.C., McIlwain, E., Lucchesi, P.A. and Varner, K.J. (2008) Ecstasy produces left ventricular dysfunction and oxidative stress in rats. *Cardiovasc. Res.*, **79**, 662–670.
29. Bruch, C., Schmermund, A., Marin, D., Katz, M., Bartel, T., Schaar, J. and Erbel, R. (2000) Tei-index in patients with mild-to-moderate congestive heart failure. *Eur. Heart J.*, **21**, 1888–1895.
30. LaCorte, J.C., Cabreriza, S.E., Rabkin, D.G., Printz, B.F., Coku, L., Weinberg, A., Gersony, W.M. and Spotnitz, H.M. (2003) Correlation of the Tei index with invasive measurements of ventricular function in a porcine model. *J. Am. Soc. Echocardiogr.*, **16**, 442–447.
31. Tei, C., Ling, L.H., Hodge, D.O., Bailey, K.R., Oh, J.K., Rodeheffer, R.J., Tajik, A.J. and Seward, J.B. (1995) New index of combined systolic and diastolic myocardial performance: a simple and reproducible measure of cardiac function—a study in normals and dilated cardiomyopathy. *J. Cardiol.*, **26**, 357–366.
32. Kitaoka, H., Takata, J., Yabe, T., Hitomi, N., Furuno, T. and Doi, Y.L. (1999) Low dose dobutamine stress echocardiography predicts the improvement of left ventricular systolic function in dilated cardiomyopathy. *Heart*, **81**, 523–527.
33. Foust, K.D., Nurre, E., Montgomery, C.L., Hernandez, A., Chan, C.M. and Kaspar, B.K. (2009) Intravascular AAV9 preferentially targets neonatal neurons and adult astrocytes. *Nat. Biotechnol.*, **27**, 59–65.
34. Pacak, C.A., Mah, C.S., Thattaliyath, B.D., Conlon, T.J., Lewis, M.A., Cloutier, D.E., Zolotukhin, I., Tarantal, A.F. and Byrne, B.J. (2006) Recombinant adeno-associated virus serotype 9 leads to preferential cardiac transduction in vivo. *Circ. Res.*, **99**, e3–9.
35. Bish, L.T., Morine, K., Sleeper, M.M., Sanmiguel, J., Wu, D., Gao, G., Wilson, J.M. and Sweeney, H.L. (2008) Adeno-associated virus (AAV) serotype 9 provides global cardiac gene transfer superior to AAV1, AAV6, AAV7, and AAV8 in the mouse and rat. *Hum. Gene. Ther.*, **19**, 1359–1368.
36. Tanaka, H., Nishi, S., Nuruki, K. and Tanaka, N. (1977) Myocardial ultrastructural changes in Kugelberg–Welander syndrome. *Br. Heart J.*, **39**, 1390–1393.
37. Huss, J.M. and Kelly, D.P. (2005) Mitochondrial energy metabolism in heart failure: a question of balance. *J. Clin. Invest.*, **115**, 547–555.
38. Lesnefsky, E.J., Moghaddas, S., Tandler, B., Kerner, J. and Hoppel, C.L. (2001) Mitochondrial dysfunction in cardiac disease: ischemia–reperfusion, aging, and heart failure. *J. Mol. Cell. Cardiol.*, **33**, 1065–1089.
39. Tanaka, H., Uemura, N., Toyama, Y., Kudo, A. and Ohkatsu, Y. (1976) Cardiac involvement in the Kugelbert–Welander syndrome. *Am. J. Cardiol.*, **38**, 528–532.
40. Kobayashi, M., Izawa, H., Cheng, X.W., Asano, H., Hirashiki, A., Unno, K., Ohshima, S., Yamada, T., Murase, Y., Kato, T.S. *et al.* (2008) Dobutamine stress testing as a diagnostic tool for evaluation of myocardial contractile reserve in asymptomatic or mildly symptomatic patients with dilated cardiomyopathy. *JACC Cardiovasc. Imaging*, **1**, 718–726.
41. Gizurarson, S., Lorentzon, M., Ramunddal, T., Waagstein, F., Bergfeldt, L. and Omerovic, E. (2007) Effects of complete heart block on myocardial function, morphology, and energy metabolism in the rat. *Europace*, **9**, 411–416.
42. Breur, J.M., Gooskens, R.H., Kapusta, L., Stoutenbeek, P., Visser, G.H., van den Berg, P. and Meijboom, E.J. (2007) Neurological outcome in isolated congenital heart block and hydrops fetalis. *Fetal Diagn. Ther.*, **22**, 457–461.
43. Breur, J.M., Kapusta, L., Stoutenbeek, P., Visser, G.H., van den Berg, P. and Meijboom, E.J. (2008) Isolated congenital atrioventricular block diagnosed in utero: natural history and outcome. *J. Matern. Fetal. Neonatal. Med.*, **21**, 469–476.
44. Olivares, J.L., Vazquez, M., Fleta, J., Moreno, L.A., Perez-Gonzalez, J.M. and Bueno, M. (2005) Cardiac findings in adolescents with anorexia nervosa at diagnosis and after weight restoration. *Eur. J. Pediatr.*, **164**, 383–386.